ACS APPLIED ENERGY MATERIALS
Cite This: ACS Appl. Energy Mater. 2018, 1, 5627−5635
Article
www.acsaem.org

Energy Harvesters Incorporating Silk from the Taiwan-Native Spider *Nephila pilipes*

Cheng-Tang Pan,[†,‡] Chung-Kun Yen,[†] Ming-Chun Hsieh,[†] Shao-Yu Wang,[†] Chi-Hui Chien,[†] Jacob Chih-Ching Huang,[⊥] Liwei Lin,[∥] Yow-Ling Shiue,[*,‡,§] and Shiao-Wei Kuo[*,⊥]

[†]Department of Mechanical and Electro-Mechanical Engineering, [‡]Institute of Medical Science and Technology, [§]Institute of Biomedical Sciences, and [⊥]Department of Materials and Optoelectronic Science, National Sun Yat-Sen University, Kaohsiung 80424, Taiwan

[∥]Department of Mechanical Engineering, University of California Berkeley, Berkeley, California 94720, United States

Supporting Information

ABSTRACT: Silks from *Nephila pilipes* spiders native to Taiwan, obtained from the major ampullate gland, display novel piezoelectric properties that have been exploited in the preparation of energy harvesters. An energy harvester incorporating approximately 100 pieces of spider silk, each approximately 10 mm long, produced a voltage output of 13.4 mV when vibrated at 4 Hz. A repolarization process enhanced the piezoelectric properties of the spider silks significantly, notably increasing the output voltage to 40.7 mV at 4 Hz. Electrical testing indicated that the output voltages of the energy harvesters incorporating the repolarized silks were 3- to 4-fold higher than those of the harvesters containing the nonpolarized silks. The maximum output power (59.5 pW) was generated by the energy harvester incorporating the repolarized silks when connected to an external load resistor of 8.2 MΩ. The mechanical properties of the spider silks were examined through both microtensile and nanoindenter tests, revealing elastic moduli between 5 and 7 GPa, strengths ranging from 510 to 850 MPa, and percentages of elongation of 20−25%. Thus, these spider silks exhibited excellent mechanical strength and ductility. Fourier transform infrared spectra of the repolarized silks revealed a significant increase in intensity and sharpening of the amide I absorption peak, suggesting that the repolarized silk proteins featured a superior arrangement of α-helices and β-sheets, relative to the nonpolarized ones. Thus, Taiwan-native *Nephila pilipes* silks, with their intrinsic piezoelectricity and good mechanical properties, exhibit great potential for use in energy harvesters.

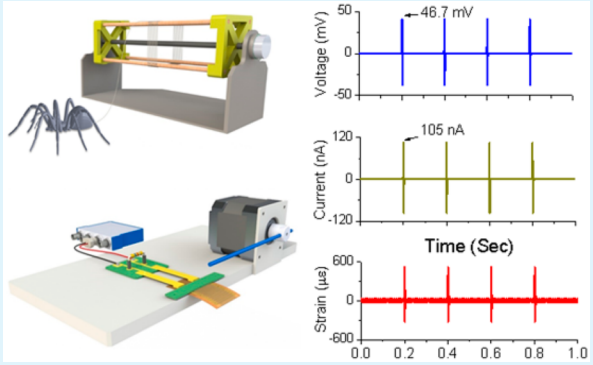

KEYWORDS: *Energy harvester, piezoelectricity, spider silk, secondary structures, polarized, Nephila Pilipes*

INTRODUCTION

Although batteries have become almost essential to our daily lives, they have several disadvantages, including limited energy storage, short life spans, and the production of chemical pollution. Many innovative technologies were studied to make energy hunting more diversified, such as piezoelectric materials and supercapacitors. Metal−organic frameworks (MOFs) can serve as high-surface-area templates to generate hierarchically ordered nanoporous carbon electrodes for supercapacitor devices; transition metal oxides (TMOs) have attracted significant attention for energy storage applications such as supercapacitors.[1−5] An alternative would be the improved development of piezoelectric devices and materials, which are self-running generators. Through the piezoelectric effect, piezoelectric materials can generate electricity upon their deformation. Moreover, the vibrational energy produced by our bodies—for example, when we walk (swinging our arms and moving our feet)—can be applied to piezoelectric materials as an efficient means of generating electricity.[6−12] In 1941, Martin et al. were the first to report piezoelectricity and related properties in biological materials.[13] In 1955, Fukada et al.[14] observed piezoelectric effects in wood, bone, and DNA. Proteins have also proved to be piezoelectric materials, based on linear coupling between their mechanical strain and electric charge as well as their crystal structures and polar orientations.[15]

Spider silks are protein fibers spun by spiders; their functions are highly dependent on their two-dimensional structures, the most common elements being α-helices and β-sheets. In an α-helix, the polypeptide chain forms a structure stabilized by intramolecular N−H and C═O hydrogen bonds, aligned almost parallel to the helical spindle, forming a high density of electric dipoles. In a β-sheet, a polypeptide chain and an adjacent chain interact through intermolecular hydrogen bonds. Spider silk proteins contain highly repetitive short sequences of

Received: July 17, 2018
Accepted: September 13, 2018
Published: September 13, 2018

DOI: 10.1021/acsaem.8b01169
ACS Appl. Energy Mater. 2018, 1, 5627−5635

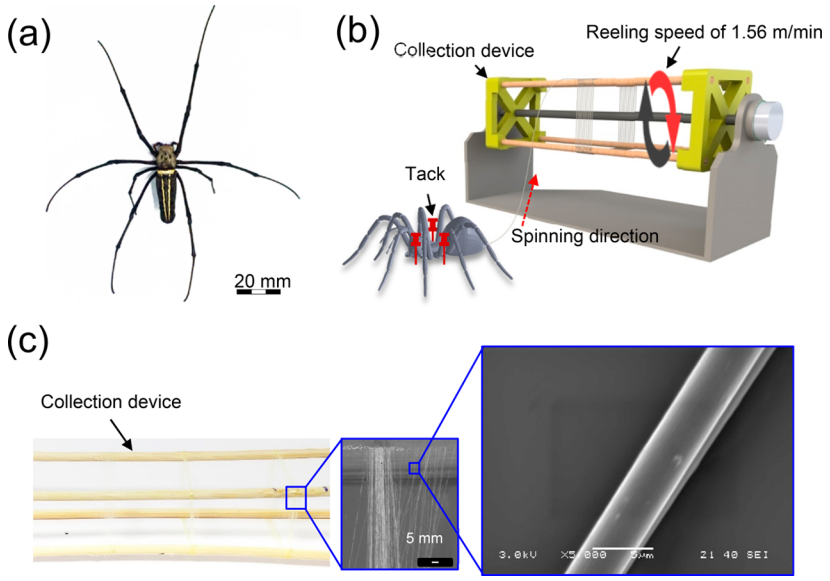

Figure 1. (a) Taiwan-native spider *Nephila pilipes*. (b) Collection of silks using a device featuring a spinning mechanism. (c) Morphology of the spider silks.

10−50 amino acids; these repetitive sequences often account for more than 90% of the protein. Each polypeptide repeat has distinct functional features that induce the outstanding mechanical properties of spider silks.[16] Furthermore, spider silks have long been used in medical applications, owing to their anti-allergic, anti-inflammatory, and biocompatible properties.[17]

Spider silks are produced by silk glands within the abdomen of the spider. A spider may have up to seven different types of silk glands (major ampullate, minor ampullate, aciniform, flagelliform, aggregate, pyriform, and cylindrical glands[18]), with the silk from each possibly functioning differently (e.g., for webbing, wrapping of prey, and lifelines to ensure safe escape from predators). Major ampullate silks are produced from the major ampullate gland; they form the frames and radii of spider webs. Accordingly, major ampullate silks are the strongest among all types of spider silks.[19] In addition to medical applications, spider silks also have potential for industrial applications that take advantage of their biocompatibility, mechanical strength, and elasticity. To the best of our knowledge, no previous reports have described the use of spider silks as energy harvesting materials. Simply understood, spider silk has a strong electrostatic force.[20] Therefore, in this study we investigated the piezoelectric effects of silks from the major ampullate gland of *Nephila pilipes*, a spider native to Taiwan.

EXPERIMENTS AND METHODS

***Nephila pilipes* Spiders.** *Nephila pilipes* spiders native to Taiwan native spiders (*Nephila pilipes*, body length: ∼ca. 3−5 cm) were used to collect silks from the major ampullate gland silks. Figure 1a displays the morphology of *Nephila pilipes*. The primary structure of the spider silks consists mainly of highly repetitive glycine and alanine blocks.[21] On the secondary structure level, the short-side-chained alanine is found mainly in the crystalline domains (β-sheets) of the nanofibrils; glycine is mostly recognized in the so-called amorphous matrix comprising helical and β-turn structures.[22] Spider silks are natural fibers made from polypeptides, which consists of α-helix, β-sheet, and amorphous chains. The combination of these proteins can be simplified into 40% ordered domains (two hydrogen bonds per amide group), 15% permanently disordered domains (one hydrogen bond per amide group), and 45% intrinsically disordered domains that may potentially become ordered. Spider silk is produced by silk glands housed within the abdomen. The major ampullate gland anatomy can be divided into three main sections: the tail, the sac, and the processing duct. The solution of the highly concentrated spider silk protein is secreted and stored inside the spinning gland. Upon initiation of thread formation, the solution is directed through a narrow ion exchange channel, in which a phase separation process takes place.

Silking Process. A female spider was sedated with carbon dioxide gas, then pinned around her limbs and abdomen, keeping her in place without causing any harm. The silk was pulled by a pair of tweezers from the spinneret, and the end of the silk was attached to the collection device and then the motor of the collection device was started to collect the silk (see Figure 1b). The silks collected here consisted mainly of major ampullate silks, which form the main structure of the web (cf. scaffolding), and minor ampullate silks, which form the main spiral of the web. The diameters of the silks were between 7 and 8 μm (Figure 1c). Afterward, the spider was released back to its web to feed, ready for the next reeling. The silk was taken at a rate of 1.6 to 3.2 mm/s by hub collector. When the silk gathering speed of silk is 1.6 mm/s, the wire diameter is evenly distributed at 8 μm (as shown in Figure 2a). When the gathering speed is increased

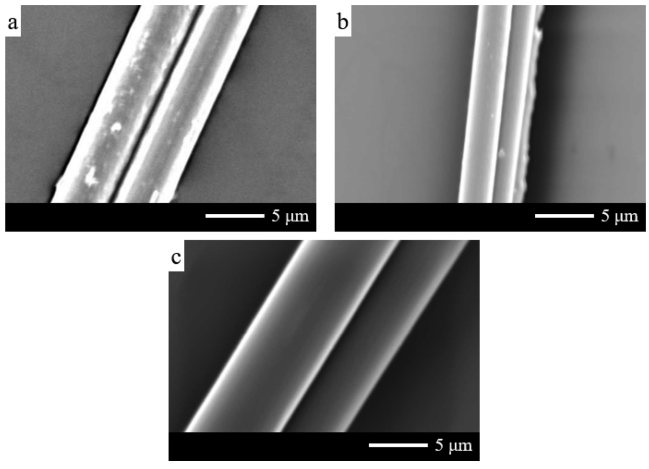

Figure 2. Surface topography and diameter of silk performance under gathering speed, (a) 1.6 mm/s, (b) 2.4 mm/s, and (c) 3.2 mm/s.

to 2.4 and 3.2 mm/s, the wire diameter is distributed between 5.3 and 2.7 μm (Figure 2b,c). However, when the gathering speed is increased

DOI: 10.1021/acsaem.8b01169
ACS Appl. Energy Mater. 2018, 1, 5627−5635

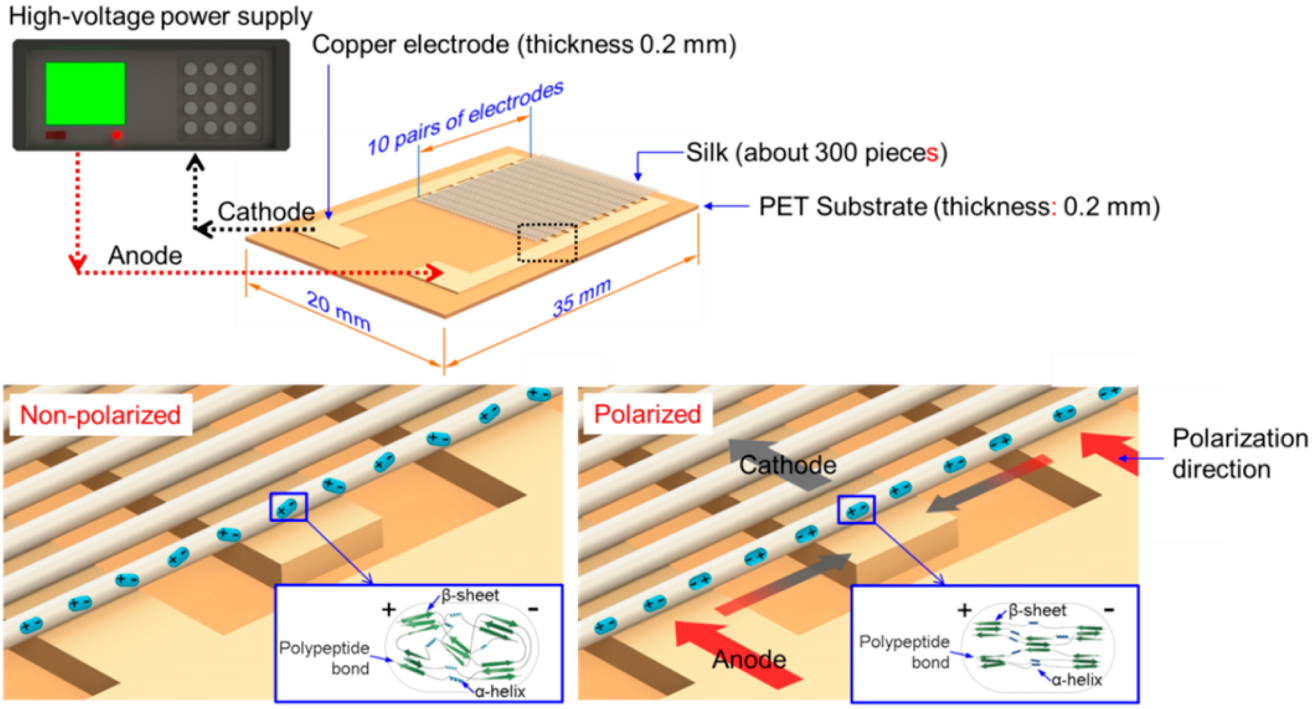

Figure 3. Repolarization of spider silks on an IDT with a gap of approximately 0.5 mm in pitch under a high voltage of 1500 V for 1 h to create a high-voltage electric field of 3×10^6 V/m.

to 3.2 mm/s, the spinning of spider silk was intermittent. When the spider's abdomen was spun under a high gathering speed, the spider could not squeeze enough water-soluble proteinogenic amino acids in a short time so that uncrystallized protein molecular chain could not be aligned, causing spider silk spinning to be interrupted.

Piezoelectric Effect. To analyze the piezoelectric effect of the spider silks, forward and backward connections were examined through a beating test. Both direct and converse piezoelectric effects were examined. In the forward connection, the positive and negative probes were connected to the positive and negative potentials, respectively, of an energy harvester made of spider silks; in the backward connection, the positive and negative probes were connected to the energy harvester in the opposite manner. The beating test was controlled using a step motor that deformed the energy harvester, inducing electrical voltage and current. The energy harvester comprising approximately 300 pieces of spider silk was packaged on a piece of flexible poly(ethylene terephthalate) (PET) with both ends connected to a copper foil electrode pair, as displayed in Figure S1. The direct piezoelectric effect is the ability to convert mechanical elastic strain energy into electrical energy. To observe the piezoelectric d_{33} mode, the spider silks were aligned perpendicular to the electrode. When a stress was applied to the energy harvester, the spider silks produced a time-dependent rate of strain along the axial direction. Because the energy harvester was deformed frequently through such beating, the deformed mechanical elastic energy was converted into an electrical voltage and current. With the piezoelectric d_{33} mode, an alternating voltage and current was generated, induced by beating the sample.

The converse piezoelectric effect involves the electricity energy being converted into deformed elastic strain energy. Figure S2(a) displays the device used to test the converse piezoelectric effect. This energy harvester was tested to verify the presence of strain deformation under an external electric field. Figure S2(b) provides a schematic representation of a packaged energy harvester used for the converse piezoelectric test. One piece of spider silk was packaged with copper electrodes, silver glue, and a polyimide film. The silver glue was applied to ensure that the silk came into complete contact with the copper electrodes. Figure S2(c) presents an optical microscopy image of spider silks in an energy harvester sample. When subjected to a high voltage field of 1.5×10^6 V/m, the spider silks were deformed and the converse piezoelectric effect were observed and characterized. Figure S2(d) reveals the experimental setup; the results were also recorded by a video camera at the same time (Figure S3(a)). The deformation was observed clearly. Figure S3(b) provides a schematic representation of the converse piezoelectric effect. The high voltage field extended the dipoles inside the spider silks and, thus, elongated the silks, leading to the converse piezoelectric effect.

Interdigitated Electrodes and Repolarization. In this study, the electrical properties of energy harvesters formed from spider silks were measured mainly using parallel electrodes. If the interspace between the parallel electrodes was too wide, the electrons in the spider silks would not be emitted and transferred from the spider silks to the electrode, due to the internal resistance of the spider silks. Therefore, an interdigitated electrode (IDT) was used to mimic the situation of many electrodes connected in parallel. The interspace of the IDT was designed to be approximately 0.5 mm.[7] A 355 nm UV laser was used to direct-write IDT patterns on the copper tape and shorten the processing time. Ten pairs of IDTs having an interspace of 0.5 mm and overall dimensions of 20 mm × 35 mm were obtained.

The spider silks (length: ca. 10 mm) were packaged on the IDT to form an energy harvester. After repolarization, the spider silks were divided into multiple groups, separated in terms of their of dipole moments. The secondary structures of the spider silks (α-helices and β-sheets) were rearranged in a more orderly manner to enhance the effect of charge addition. Using this IDT structure, the energy harvester was divided into multiple smaller energy harvesting cells. As displayed in Figure 3, spider silks were subjected to the repolarization process to compare the resulting piezoelectric properties with those of nonpolarized spider silks. The spider silks attached on the IDT with a gap of approximately 0.5 mm were maintained under a high voltage of 1500 V for 1 h to create a high voltage electric field of 3×10^6 V/m.

Energy Harvesting. The observed direct and converse piezoelectric effects revealed that the spider silks in the energy harvester behaved as piezoelectric materials. Nevertheless, the spider silks themselves exhibited considerable intrinsic impedance. Impedance matching (i.e., matching the load impedance and internal impedance) would, therefore, become necessary to maximize the poweroutput. Different circuit designs can vary the impedance matching conditions. Figure 4 displays the impedance matching circuit used in this study; the electrical source and elements for the spider silks are presented schematically.

DOI: 10.1021/acsaem.8b01169
ACS Appl. Energy Mater. 2018, 1, 5627−5635

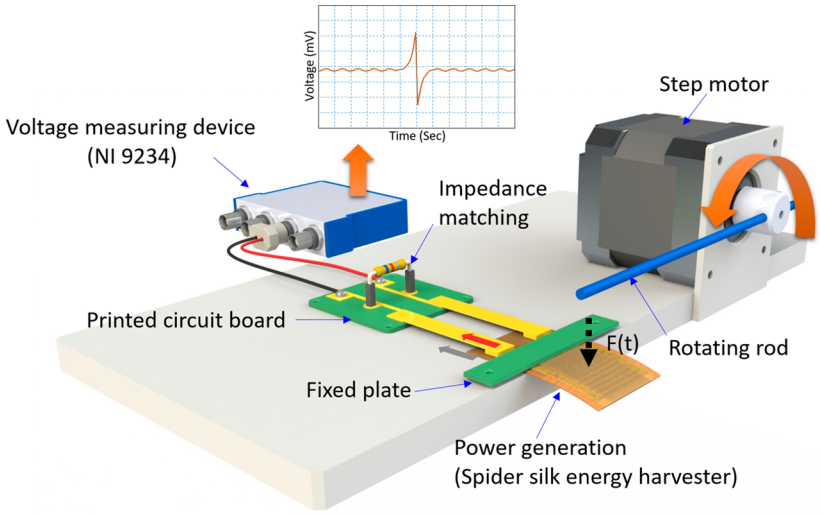

Figure 4. Impedance matching circuit with an electrical source and elements for the energy harvester and representation of the measurement method after performing the impedance matching process.

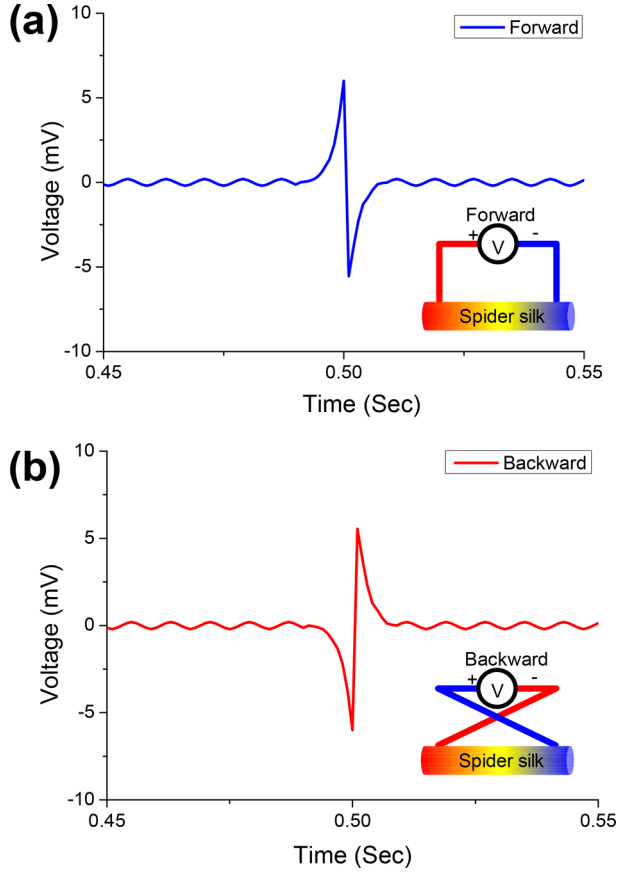

Figure 5. Comparison of voltage signals obtained from a harvester connected in (a) forward and (b) backward modes.

Measurement of Mechanical Strength. The mechanical properties of the spider silks were investigated using microtensile and nanoindentation tests. A 250-N load cell was used as the force sensor to perform the microtensile test. Stress and strain were measured from the load and displacement of the spider silks. A stress−strain curve was drawn to obtain the Young's modulus, maximum tensile strength, and percentage of elongation. For the nanoindentation test, one probe with a specific force was designed to indent the spider silks. Once the force on the probe was released, an indentation was formed on the spider silk. The measured force and indentation area were converted into the Young's modulus. The nanoindentation system employed was a Hysitron nanoindenter (Figure S4(a)); the experimental platform included the probe, positioning stage, and optical microscope (Figure S4(b)). Figure S4(c) depicts the energy harvester, formed from spider silks, on a holder, fixed on an aluminum rod, that was used for the nanoindenter test.

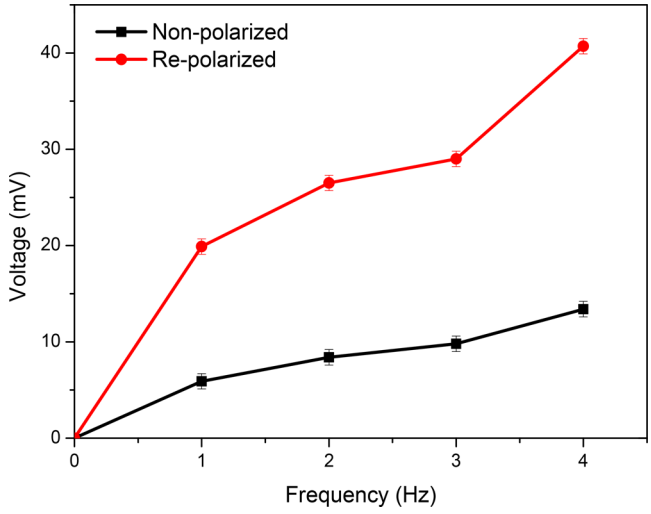

Figure 6. Comparison of voltage output responses from the nonpolarized and repolarized energy harvesters at beating frequencies from 1 to 4 Hz about voltage output.

FTIR Spectroscopy. FTIR spectra were recorded to investigate the structural differences between the nonpolarized and repolarized spider silks. The characteristic signals and wavenumbers of the absorption peaks were used to decipher the molecular structure and orientation of the spider silks. Potassium bromide (KBr) powder was added to samples of the nonpolarized and repolarized spider silks. The powders were pressurized into tablets, using an oil hydraulic press, and loaded into the spectrometer. The energy absorptions of the spider silks were further measured using an infrared light sensor. Scanning electron microscopy (SEM) was used to observe the surface morphologies and diameters of the spider silks.

RESULTS AND DISCUSSION

During the silking process, mechanical drawing of the silk thread (hind legs/gravity) results in rapid assembly of the silk fibers. Starting with an almost entire random coil structure in

DOI: 10.1021/acsaem.8b01169
ACS Appl. Energy Mater. 2018, 1, 5627−5635

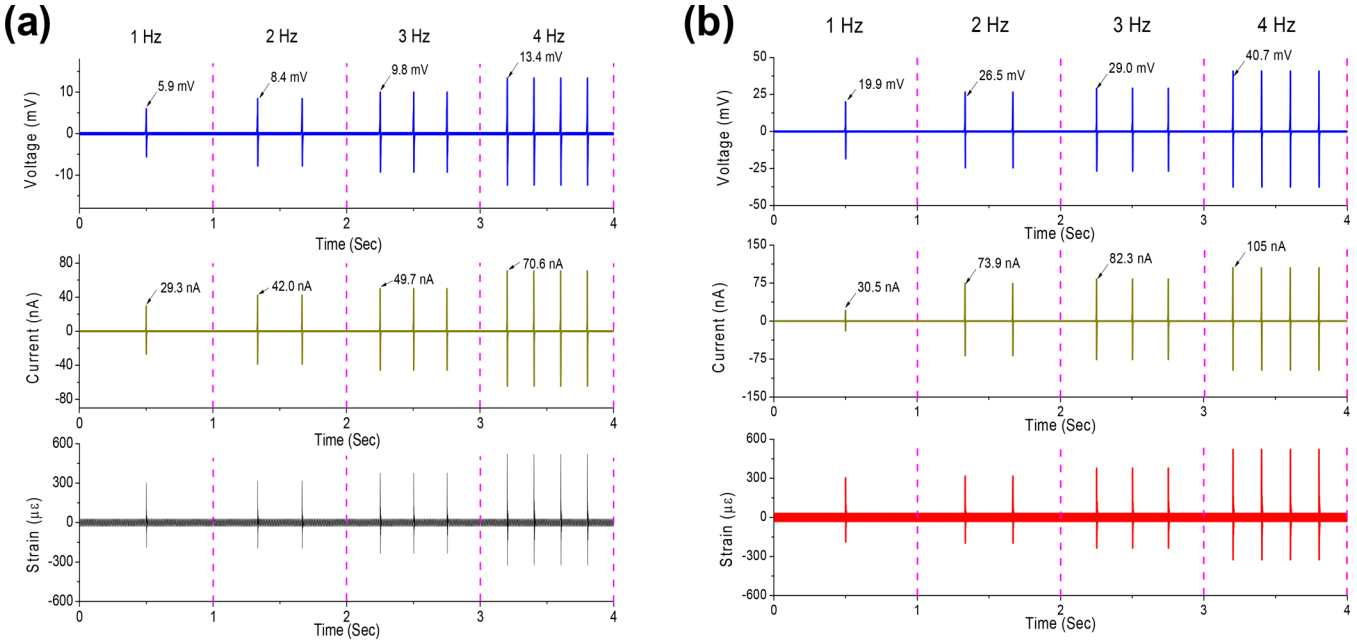

Figure 7. Comparison of voltage, current, and strain output responses from the nonpolarized and repolarized energy harvesters at beating frequencies from 1 to 4 Hz: (a) nonpolarized, (b) repolarized.

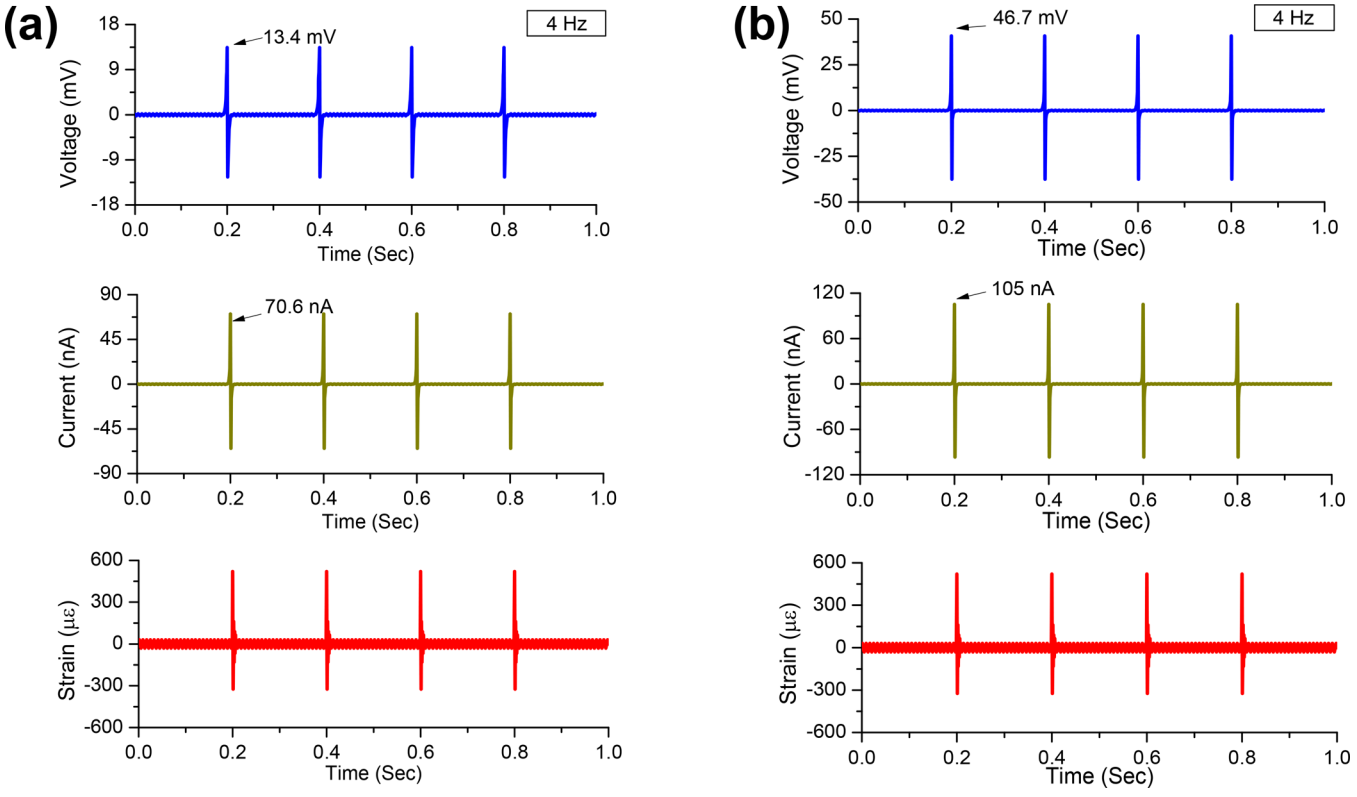

Figure 8. Comparison of voltage, current, and strain output responses, at single 4 Hz, from the (a) nonpolarized and (b) repolarized energy harvester.

the gland, silk proteins rapidly assemble upon passage through the spinning duct and the silk structure becomes water-insoluble. The tightly controlled assembly behavior requires bistable folding of the involved protein and optimal environments in the spinning duct (e.g., pH, ionic concentration, water content). Two existing theories explain the molecular process occurring inside the spinning duct. One supports a liquid-crystalline behavior of the silk proteins, whereas the other favors micellar organization of the proteins, before elongation (through laminar force) finally leads to thread assembly.[23]

Piezoelectric effects. *1. Nonpolarized Silks.* SEM images revealed that the spider silks in the energy harvester were smooth and had diameters between 6.5 and 8 μm. Beating tests confirmed that the energy harvester could convert mechanical

DOI: 10.1021/acsaem.8b01169
ACS Appl. Energy Mater. 2018, 1, 5627−5635

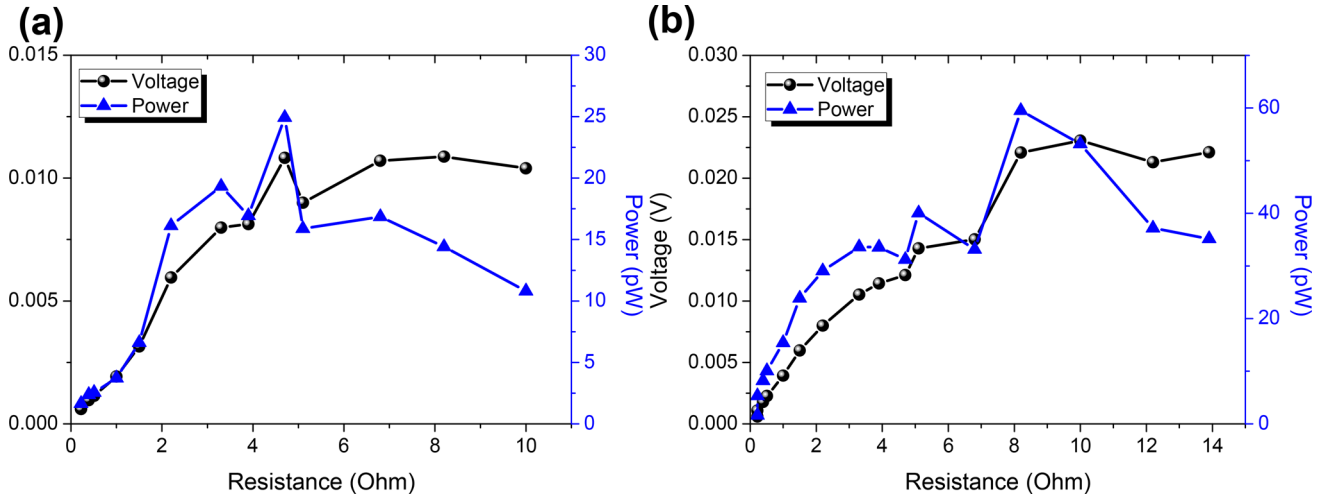

Figure 9. Maximum power outputs of energy harvesters: (a) nonpolarized silks (24.9 pW; 4.7 MΩ external resistor); (b) repolarized silks (59.5 pW; 8.2 MΩ external resistor).

strain energy into electrical energy, measured in terms of voltage and current outputs. Before performing a beating test, the energy harvester was attached to a sensor to detect the electrical signal wave and verify the polarity direction, with both forward and backward connections (Figure 5). In the forward connection, the positive and negative probes were connected to the positive and negative potentials, respectively, of the energy harvester. When a beating test was performed with an applied vibration of 1 Hz, electrical outputs were generated (Figure 5(a)). In the backward connection, when a beating test was performed with a 1 Hz vibration, the opposite electrical signal was generated. Because the polarity direction of the spider silks in the energy harvester was fixed orientationally, when the energy harvester was connected in the reverse manner the response output was generated with the opposite waveform (cf. Figures 5(b) and 4(a)). Next, to analyze the effects of various beating frequencies on the signal outputs, we deformed the packaged energy harvester under low-frequency beating vibrations (1−4 Hz) and measured the voltage, current, and strain. At frequencies of 1, 2, 3, and 4 Hz, the output voltages of the nonpolarized spider silks in the energy harvester were approximately 5.9, 8.4, 9.8, and 13.4 mV, respectively (Figure 6). Thus, higher beating frequencies did indeed result in larger voltage outputs.

2. Repolarized Silks. Using IDT structures, we divided 10-mm-long spider silks into the multiple cells of smaller energy harvesters. After repolarization treatment of the spider silks, they were partitioned into multiple groups, separated in terms of their dipole moments. The piezoelectric properties of the energy harvesters incorporating the repolarized spider silks were notably improved. To determine the effect of repolarization on the signal output, again we deformed the energy harvesters under various beating vibration frequencies from 1 to 4 Hz and measured their voltage, current, and strain. The output voltages of the repolarized spider silk energy harvester increased from 19.9 to 40.7 mV upon increasing the frequency from 1 to 4 Hz (Figure 6). Figure 7(a,b) compares the electrical and mechanical responses from the nonpolarized and repolarized energy harvesters, respectively, at these frequencies. At a beating frequency of 4 Hz, the nonpolarized energy harvester generated a voltage output of 13.4 mV, a current of 70.6 nA, and strain rate of 0.0575 s^{-1} (Figure 8(a)); for the repolarized energy harvester, these values were 40.7 mV, 105 nA, and 0.0575 s^{-1}, respectively (Figure 8(b)). Thus, repolarization of the energy harvester caused the voltage and current to increase significantly, by 3.5- and 1.5-fold, respectively. We attribute the significant increases in the electrical outputs of the repolarized energy harvester to the high-voltage electric field having induced further directional arrangement of the internal dipoles, thereby enhancing the piezoelectric effect.

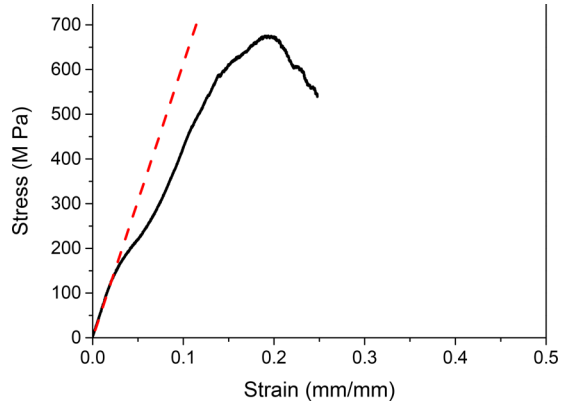

Figure 10. Young's moduli of spider silks, measured between 5 and 7 GPa, determined using a microtensile tester with a gage length of 15 mm.

Power Generation. We performed an impedance matching test to obtain the maximum power output in the case where the external load resistance was equal to the internal resistance. The energy harvester incorporating the nonpolarized spider silks generated a maximum output power of 24.9 pW when connected to a 4.7 MΩ external resistor (Figure 9(a)), whereas the energy harvester made of repolarized spider silks generated a maximum output power of 59.5 pW when connected to a 8.2 MΩ external resistor (Figure 9(b)).

Mechanical Strength. We used a microtensile tester having a gauge length of 15 mm to characterize the mechanical strength of the spider silks. Figure 10 reveals that the Young's modulus of the spider silks was between 5 and 7 GPa, the strength ranged from 510 to 850 MPa, and the percentage of elongation was 20−25%. A nanoindentation test conducted on the spider silks suggested that the Young's modulus of the spider silks was between 5.7 and 7 GPa (Figure 11), similar to the range

DOI: 10.1021/acsaem.8b01169
ACS Appl. Energy Mater. 2018, 1, 5627−5635

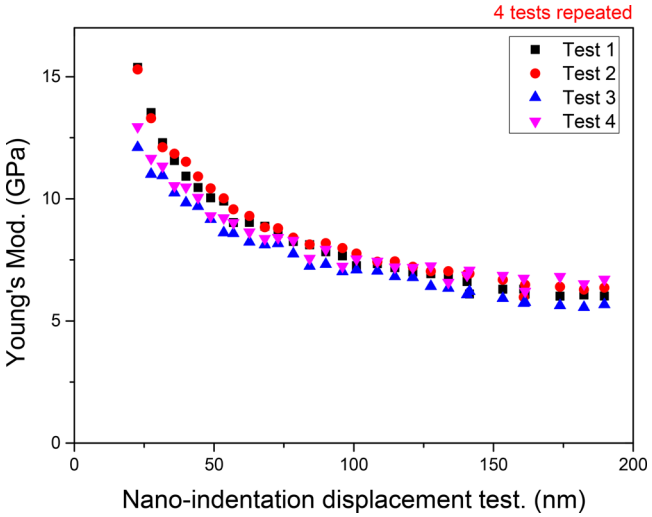

Figure 11. Young's moduli of spider silks, measured between 5.7 and 7 GPa, determined through nanoindentation.

Table 1. Mechanical Properties of Dragline Silks from Spiders, Silkworm Silk, and Kevlar

Silk type	Young's modulus (GPa)	Strength (MPa)	Elongation (%)
Nephila pilipes	5.5	627	22.3
Nephila clavipes[24]	13.8	1215	17.2
Gasteracantha cancriformis[24]	7.3	1199	33.1
Deinopis spinose[24]	10.4	1345	19.1
Latrodectus geometricus[24]	10.2	764	31
Latrodectus hesperus[25]	10.2	1441	30.3
Caerostris darwini[26]	11.5	1652	52
Bombyx mori (silkworm)[27]	5	600	18
Kevlar[27]	100	4000	3.9

obtained from the microtensile tests (i.e., the measured mechanical properties were similar when using micro- and nanoscale equipment). Moreover, compared with the silk fibers obtained from spiders from other areas (Table 1), the silk from the Taiwan-native *Nephila pilipes* spider was slightly lower in mechanical strengths, presumably an innate characteristic of this spider species. Nevertheless, the spider silks exhibited good mechanical strength and ductility.

FTIR Spectroscopy. We recorded FTIR spectra to identify any variations in molecular bonding in the nonpolarized and repolarized spider silks. Figure 12a displays the FTIR spectra (4000−400 cm^{-1}) of the spider silks, recorded at room temperature. The spectrum of the repolarized spider silks featured a significant signal at 1385 cm^{-1}, and suggested a better crystal arrangement than that of the nonpolarized silks. Notably, the piezoelectric effect of the repolarized spider silks was better than that of the nonpolarized ones. We further analyzed these spectra using the second derivative method,[28−31] considering the signals for amide I (CONH) stretching in the range 1600−1700 cm^{-1} (Figure 12(b)). The secondary structures of the spider silks consisted of aggregated strands (signal at 1610 cm^{-1}), parallel β-sheets (signals at 1620, 1630, and 1695 cm^{-1}), random coils (signals at 1641 and 1651 cm^{-1}), α-helices (signals at 1651 and 1659 cm^{-1}), and β-turns (signals at 1668, 1673, and 1682 cm^{-1}), based on the curve-fitted data using the second derivative method. We used the second derivative curve of the amide I spectrum to determine the positions of the deconvoluted peaks. The content of the α-helix conformation of the repolarized spider silks had increased by approximately 3% relative to that of the nonpolarized spider silks. We suspect that it was mainly the α-helices in the silk proteins that contributed to the piezoelectric properties. Accordingly, the piezoelectric effect of the spider silks increased after performing the repolarization process.

CONCLUSION

We have explored the use of natural spider silks as a novel energy harvesting material. The diameters of the tested spider silks were between 6.5 and 8 μm, with smooth surfaces. The measured Young's moduli, strengths, and elongation percentages of the spider silks were in the ranges 5−7 GPa, 510−850 MPa, and 20−25%, respectively. A nanoindentation test revealed that the Young's modulus of the spider silks was similar to that identified using a microtensile tester. The energy harvester

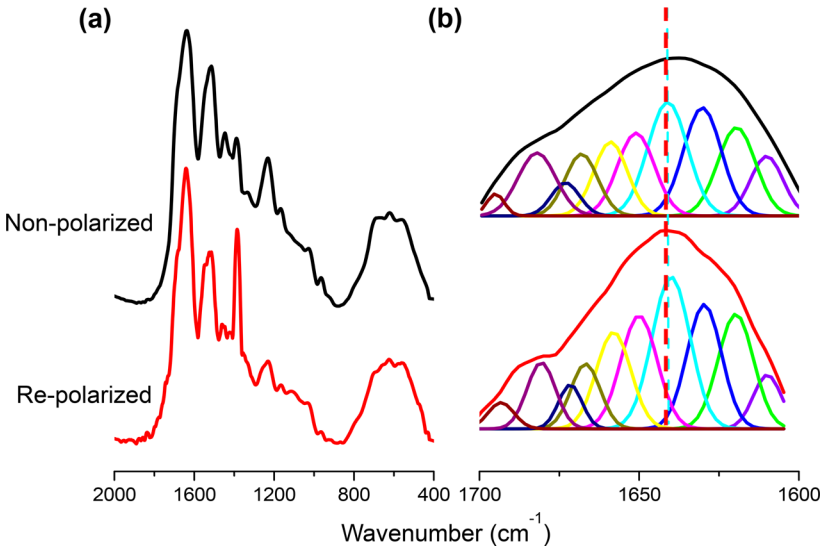

Figure 12. (a) FTIR spectra of nonpolarized and repolarized spider silk harvesters. (b) FTIR spectral analysis between 1600 and 1700 cm^{-1}, performed using the second derivative method.

DOI: 10.1021/acsaem.8b01169
ACS Appl. Energy Mater. 2018, 1, 5627−5635

made of spider silks converted the mechanical strain energy from beating into electrical energy, measured in terms of voltage and current outputs. Therefore, the piezoelectric effect of these spider silks was substantiated. The electrical properties of the energy harvester were determined using IDT electrodes, which revealed that repolarization improved the electrical output. The voltage outputs of the energy harvester incorporating the repolarized spider silk increased from 19.9 to 40.7 mV upon increasing the beating frequency from 1 to 4 Hz. These voltage outputs were enhanced significantly, by 3- to 4-fold, relative to those of the harvested containing the nonpolarized silks. The energy harvester with the repolarized spider silks generated a maximum power output of 59.5 pW when connected to an 8.2 MΩ external resistor. The content of α-helix conformations in the spider silks increased by approximately 3% after repolarization treatment; it appears that it is the α-helices that contribute the main piezoelectric properties to proteins. In this study, we used only approximately 100 pieces of spider silk, each approximately 10 mm long, to prepare the energy harvesters. If more power is needed, we should be able to scale up the silk counts to obtain higher electrical voltages and higher power outputs. Thus, spider silks have great potential for use as energy harvesters or as sensor, due to their intrinsic piezoelectricity.

■ ASSOCIATED CONTENT

Supporting Information

The Supporting Information is available free of charge on the ACS Publications website at DOI: 10.1021/acsaem.8b01169.

Powering process and measurement devices for an energy harvester, the structure of spider silk, the deformation of spider silk and dipole effect of spider silks, the nanoindentation test of spider silks, and the electrical properties of the nonpolarized and repolarized energy harvesters (PDF)

■ AUTHOR INFORMATION

Corresponding Authors

*E-mail: shirley@imst.nsysu.edu.tw.

*E-mail: kuosw@faculty.nsysu.edu.tw.

ORCID

Shiao-Wei Kuo: 0000-0002-4306-7171

Notes

The authors declare no competing financial interest.

■ ACKNOWLEDGMENTS

This study was supported financially by the Ministry of Science and Technology, Taiwan, under contra MOST 106-2221-E-110-067-MY3 and 105-2221-E-110-092- MY3.

■ REFERENCES

(1) Salunkhe, R. R.; Lee, Y. H.; Chang, K. H.; Li, J. M.; Simon, P.; Tang, J.; Torad, N. L.; Hu, C. C.; Yamauchi, Y. Nanoarchitectured Graphene Based Supercapacitors for Next Generation Energy Storage Applications. *Chem. - Eur. J.* **2014**, *20*, 13838−13852.

(2) Salunkhe, R. R.; Hsu, S. H.; Wu, K. C. W.; Yamauchi, Y. Large-Scale Synthesis of Reduced Graphene Oxides with Uniformly Coated Polyaniline for Supercapacitor Applications. *ChemSusChem* **2014**, *7*, 1551−1556.

(3) Salunkhe, R. R.; Tang, J.; Kobayashi, N.; Kim, J.; Ide, Y.; Tominaka, S.; Kim, J. H.; Yamauchi, Y. Ultrahigh Performance Supercapacitors Utilizing Core-Shell Nanoarchitectures from A Metal-Organic Framework-Derived Nanoporous Carbon and A Conducting Polymer. *Chem. Sci.* **2016**, *7*, 5704−5713.

(4) Salunkhe, R. R.; Kaneti, Y. V.; Yamauchi, Y. Metal-Organic Framework-Derived Nanoporous Metal Oxides toward Supercapacitor Applications: Progress and Prospects. *ACS Nano* **2017**, *11*, 5293−5308.

(5) Young, C.; Wang, J.; Kim, J.; Sugahara, Y.; Henzie, J.; Yamauchi, Y. Controlled Chemical Vapor Deposition for Synthesis of Nanowire Arrays of Metal-Organic Frameworks and Their Thermal Conversion to Carbon/Metal Oxide Hybrid. *Chem. Mater.* **2018**, *30* (10), 3379−3386.

(6) Fang, J.; Niu, H.; Wang, H.; Wang, X.; Lin, T. Enhanced Mechanical Energy Harvesting Using Needleless Electrospun Poly(vinylidene fluoride) Nanofibre Webs. *Energy Environ. Sci.* **2013**, *6*, 2196−2202.

(7) Zhang, H.; Yang, Y.; Su, Y.; Chen, J.; Adams, K.; Lee, S.; Hu, C.; Wang, Z. L. Triboelectric Nanogenerator for Harvesting Vibration Energy in Full Space and As Self-Powered Acceleration Sensor. *Adv. Funct. Mater.* **2014**, *24*, 1401−1407.

(8) Pan, C. T.; Yen, C. K.; Lin, L.; Lu, Y. S.; Li, H. W.; Huang, J. C. C.; Kuo, S. W. Energy Harvesting With Piezoelectric Poly(γ-benzyl-L-glutamate) Fibers Prepared Through Cylindrical Near-Field Electrospinning. *RSC Adv.* **2014**, *4*, 21563−21570.

(9) Pan, C. T.; Yen, C. K.; Wu, H. C.; Lin, L.; Lu, Y. S.; Huang, J. C. C.; Kuo, S. W. Significant Piezoelectric and Energy Harvesting Enhancement of Poly(vinylidene fluoride)/Polypeptide Fiber Composites Prepared Through Near-Field Electrospinning. *J. Mater. Chem. A* **2015**, *3*, 6835−6843.

(10) Pan, C. T.; Yen, C. K.; Wang, S. Y.; Lai, Y. C.; Lin, L.; Huang, J. C. C.; Kuo, S. W. Near-Field Electrospinning Enhances the Energy Harvesting of Hollow PVDF Piezoelectric Fibers. *RSC Adv.* **2015**, *5*, 85073−85081.

(11) Marino, A.; Genchi, G. G.; Sinibaldi, E.; Ciofani, G. Piezoelectric Effects of Materials on Bio-Interfaces. *ACS Appl. Mater. Interfaces* **2017**, *9*, 17663−17680.

(12) Yang, E.; Xu, Z.; Chur, L. K.; Behroozfar, A.; Baniasadi, M.; Mereno, S.; Huang, J.; Gilligan, J.; Jolandan, M. M. Nanofibrous Smart Fabrics from Twisted Yarns of Electrospun Piezopolymer. *ACS Appl. Mater. Interfaces* **2017**, *9*, 24220−24229.

(13) Martin, A. J. P. Tribo-Electricity in Wool and Hair. *Proc. Phys. Soc.* **1941**, *53*, 186.

(14) Eiichi, F. Piezoelectricity of Wood. *J. Phys. Soc. Jpn.* **1955**, *10*, 149−154.

(15) Denning, D.; Alilat, S.; Habelitz, S.; Fertala, A.; Rodriguez, B. J. Visualizing Molecular Polar Order in Tissues via Electromechanical Coupling. *J. Struct. Biol.* **2012**, *180*, 409−419.

(16) Lewis, R. V. Spider Silk: Ancient Ideas for New Biomaterials. *Chem. Rev.* **2006**, *106*, 3762−3774.

(17) Gellynck, K.; Verdonk, P.; Forsyth, R.; Almqvist, K. F.; van Nimmen, E.; Gheysens, T.; Mertens, J.; van Langenhove, L.; Kiekens, P.; Verbruggen, G. Biocompatibility and Biodegradability of Spider Egg Sac Silk. *J. Mater. Sci.: Mater. Med.* **2008**, *19*, 2963.

(18) Hu, X.; Yang, J.; Wang, X.; Vasanthavada, K.; Falick, A. M.; Jone, P. R.; Mattina, C. L.; Vierra, C. A. Analysis of Aqueous Glue Coating Proteins on the Silk Fibers of the Cob Weaver, Latrodectus hesperus. *Biochemistry* **2007**, *46*, 3294−3303.

(19) Romer, L.; Scheibel, T. The Elaborate Structure of Spider Silk: Structure and Function of A Natural High Performance Fiber. *Prion* **2008**, *2*, 154−161.

(20) Morley, E. L.; Robert, D. Electric Fields Elicit Ballooning in Spiders. *Curr. Biol.* **2018**, *28* (14), 2324−2330.

(21) Simmons, A.; Michal, C. A.; Jelinski, L. W. Molecular Orientation and Two-Component Nature of the Crystalline Fraction of Spider Dragline Silk. *Science* **1996**, *271*, 84−87.

(22) Van Beek, J. D.; Hess, S.; Vollrath, F.; Meier, B. H. The Molecular Structure of Spider Dragline Silk: Folding and Orientation of the Protein Backbone. *Proc. Natl. Acad. Sci. U. S. A.* **2002**, *99*, 10266−10271.

DOI: 10.1021/acsaem.8b01169
ACS Appl. Energy Mater. 2018, 1, 5627−5635

(23) Brown, C. P.; et al. With Great Structure Comes Great Functionality: Understanding and Emulating Spider Silk. *J. Mater. Res.* **2015**, *30*, 108−120.
(24) Boutry, A. C.; Blackledge, T. A. Spider Silk Aging: Initial Improvement in A High Performance Material Followed by Slow Degradation. *J. Exp. Zool., Part A* **2008**, *309A*, 494−504.
(25) Kuntner, A. M.; Blackledge, T. A. Bioprospecting Finds the Toughest Biological Material: Extraordinary Silk from a Giant Riverine Orb Spider. *PLoS One* **2010**, *5*, e11234.
(26) Swanson, B. O.; Blackledge, T. A.; Summers, A. P.; Hayashi, C. Y. Spider Dragline Silk: Correlated and Mosaic Evolution in High-Performance Biological Materials. *Evolution* **2006**, *60*, 2539−2551.
(27) Asrar, I.; Hill, J. C. Biosynthetic Processes for Linear Polymers. *J. Appl. Polym. Sci.* **2002**, *83*, 457−483.
(28) Metwalli, E.; Slotta, U.; Darko, C.; Roth, S. V.; Scheibel, T.; Papadakis, C. M. Structural Changes of Thin Films from Recombinant Spider Silk Proteins Upon Post-Treatment. *Appl. Phys. A: Mater. Sci. Process.* **2007**, *89*, 655−661.
(29) Chen, X.; Knight, D. P.; Shao, Z.; Vollrath, F. Conformation Transition in Silk Protein Films Monitored by Time-Resolved Fourier Transform Infrared Spectroscopy: Effect of Potassium Ions on *Nephila* Spidroin Films. *Biochemistry* **2002**, *41*, 14944−14950.
(30) Kuo, S. W.; Chen, C. J. Using Hydrogen-Bonding Interactions To Control the Peptide Secondary Structures and Miscibility Behavior of Poly(L-glutamate)s with Phenolic Resin. *Macromolecules* **2011**, *44*, 7315−7326.
(31) Mohamed, M. G.; Lu, F. H.; Hong, J. L.; Kuo, S. W. Strong Emission of 2, 4, 6-Triphenylpyridine-Functionalized p = Polytyrosine and Hydrogen-Bonding Interactions with Poly (4-vinylpyridine). *Polym. Chem.* **2015**, *6*, 6340−6350.

DOI: 10.1021/acsaem.8b01169
ACS Appl. Energy Mater. 2018, 1, 5627−5635